Controlling the magnetic anisotropy in epitaxial $Y_3Fe_5O_{12}$ films by manganese doping

C. T. Wang,[1,2,3] X. F. Liang,[4] Y. Zhang,[1,2,3] X. Liang,[1,2,3] Y. P. Zhu,[1,2,3] J. Qin,[1,2,3] Y. Gao,[5] B. Peng,[1,2,3] N. X. Sun,[4] and L. Bi[1,2,3,*]

[1]*National Engineering Research Center of Electromagnetic Radiation Control Materials, University of Electronic Science and Technology of China, Chengdu 610054, China*

[2]*State Key Laboratory of Electronic Thin Films and Integrated Devices, University of Electronic Science and Technology of China, Chengdu 610054, China*

[3]*Key Laboratory of Multi-spectral Absorbing Materials and Structures of Ministry of Education, University of Electronic Science and Technology of China, Chengdu 610054, China*

[4]*Department of Electrical and Computer Engineering, Northeastern University, 360 Huntington Avenue, Boston, Massachusetts 02115, USA*

[5]*Winchester Technologies, LLC, Burlington, Massachusetts, 01803, USA*

(Received 13 June 2017; revised manuscript received 11 October 2017; published 1 December 2017)

Controlling the magnetic anisotropy in epitaxial $Y_3Fe_5O_{12}$ (YIG) thin films is critical for magnonic and photonic device applications. In this paper, we report the crystal structure, magnetic properties, and magnetic anisotropy of epitaxial $Y_3(Fe_{5-x}Mn_x)O_{12}$ (Mn:YIG) thin films grown on $Gd_3Ga_5O_{12}$ (111) (GGG) substrates by pulsed-laser deposition. Mn doping is observed to strongly enhance the magnetoelastic coefficient of YIG thin films, which leads to large tunability of the thin film magnetic anisotropy by lattice strain. With increasing Mn concentration from $x = 0$ to $x = 1.25$, a continuous increase of out-of-plane magnetic anisotropy ranging from -644.4 Oe to 1337.5 Oe is observed. In particular, a perpendicular magnetic anisotropy (PMA) is achieved in Mn:YIG thin films with a high Mn concentration of $x = 1.12$. Ferromagnetic resonance (FMR) measurements show low FMR linewidths of 3.4 Oe to 129 Oe at 9.5 GHz in Mn:YIG thin films. Our paper demonstrates manganese doping as an effective way to enhance the magnetoelastic anisotropy of YIG thin films by strain, which is useful for magnonic and magneto-optical device applications.

DOI: 10.1103/PhysRevB.96.224403

Due to the room temperature ferrimagnetic property, low optical loss, and low Gilbert damping coefficient, $Y_3Fe_5O_{12}$ (YIG) thin films have attracted significant research interest for magneto-optical and magnonic device applications. In YIG thin films, the magnetic anisotropy is dominated by the shape anisotropy with the magnetization easy axis lying in the film plane. For magnonic applications, it is important to have controllable magnetic anisotropy in YIG thin films while maintaining low damping. In particular, a perpendicular magnetic anisotropic YIG thin film with out-of-plane (OP) magnetization easy axis is useful for spin polarizer [1], spin-torque oscillator [2], spin-transfer-torque device [3], and magneto-optical device applications [4]. One way to tune the magnetic anisotropy of YIG thin films is to utilize the lattice distortion and magnetoelastic effect [5–7]. For example, by controlling the lattice strain in epitaxial YIG thin films grown on yttrium aluminum garnet (YAG) substrates with different thicknesses, it is demonstrated that the OP anisotropy of YIG thin films is proportional to the lattice tetragonality. An OP uniaxial anisotropy field of $H_{2\perp} = -1250$ Oe has been observed in 9.8 nm YIG thin films on YAG [8]. Thermal strain has also been observed to cause perpendicular magnetic anisotropy (PMA) in 10 nm polycrystalline YIG films deposited on quartz substrates due to the different thermal expansion coefficients between YIG ($10.4 \times 10^{-6}\,K^{-1}$) and quartz ($0.5 \times 10^{-6}\,K^{-1}$) [9]. However, a relatively large strain is required to tune the magnetic anisotropy of YIG thin films in these studies, which limits the observation of PMA behavior in thicker YIG films. This is essentially due to the d^5 electron configuration of Fe^{3+} ions. The almost quenched orbital momentum of the half-full d shell in Fe^{3+} leads to weak spin-orbital coupling of this material; therefore, pure YIG shows a very low magnetoelastic constant of -2.22×10^{-6} [10]. To overcome this issue, doping YIG with strong spin-orbit coupling ions has also been proved to induce controllable magnetic anisotropy [11]. For example, PMA properties have been reported in both Bi^{3+}, Dy^{3+} co-doped YIG thin films [12] and $Tm_3Fe_5O_{12}$ thin films [13].

Mn^{3+} as a Jahn-Teller ion has also been used to control the magnetoelastic constant of magnetic oxides. The d^4 configuration of Mn^{3+} ions induces strong orbit-lattice coupling in oxygen octahedrons due to their half-filled e_g orbitals, which leads to spontaneous lattice distortion and strong magnetoelastic anisotropy in Mn doped perovskites [14] or spinel magnetic oxides [15]. Mn^{3+} doping in YIG bulk materials has also been reported in previous studies [16,17]. However, systematic study on the magnetic anisotropy of YIG thin film on Mn^{3+} element doping, especially on the high Mn concentration side, has not been investigated so far. Given that Mn^{3+} is a strong magnetoelastic ion [16], the magnetic anisotropy of Mn doped YIG (Mn:YIG) epitaxial thin films should be more sensitive to lattice distortion compared to YIG, making it a promising approach to tailor the magnetic anisotropy in epitaxial Mn:YIG thin films.

In this paper, we report a study on the magnetic anisotropy of Mn:YIG thin films epitaxially grown on GGG(111) substrates by pulsed-laser deposition (PLD). Mn:YIG thin films show tunable OP magnetic anisotropy as a function of Mn concentrations and lattice strains. In particular, PMA is observed in thin films with Mn concentration of $x = 1.12$. The Mn:YIG thin films also show narrow ferromagnetic resonance

*Corresponding author: bilei@uestc.edu.cn

(FMR) linewidths ranging from 3.4 Oe to 129 Oe, which is promising for magnonic device applications.

Mn:YIG thin films were epitaxially grown on GGG(111) substrates by PLD using a COMPex Pro 205F KrF excimer laser source ($\lambda = 248$ nm). A combinatorial growth process was used to control the Mn concentrations, i.e., the laser ablates two targets of $Y_3Fe_5O_{12}$ and $Y_3Mn_2Fe_3O_{12}$ in an alternative way. By controlling the total pulses on each target, films with Mn concentrations of $x = 0.69$, 0.84, 0.97, 1.12, and 1.25 were deposited, namely Mn069, Mn084, Mn097, Mn112, and Mn125, respectively. The films' compositions were measured by x-ray photoluminescence spectroscopy (XPS, Thermo Scientific ESCALAB 250Xi). For all film growth conditions, the pulse frequency was kept at 10 Hz, and the fluence was 2.5 J/cm^2. Before deposition, the chamber was evacuated to a base pressure of 1.5×10^{-6} Torr. The oxygen partial pressure was maintained at 100 mTorr, and the substrate temperature was controlled at 800 °C during deposition. After deposition, the chamber was fluxed with 10 Torr oxygen partial pressure, and the samples were cooled down to room temperature with a cooling rate of 5 °C/ min. Film thicknesses of YIG, Mn069, Mn084, Mn097, Mn112, and Mn125 were 203 nm, 217 nm, 219 nm, 225 nm, 227 nm, and 230 nm, respectively, as measured by cross-sectional scanning electron microscopy (SEM: JEOL JSM7600F). The crystal structure of Mn:YIG thin films was studied by x-ray diffraction (XRD, Jordan Valley D1 Evolution). Both the ω-2θ scan and reciprocal space map (RSM) were measured on all samples to evaluate the Mn:YIG lattice structure. The x-ray wavelength of XRD and RSM measurements is 0.15406 nm. The atomic force microscopy (AFM) measurements were characterized by tapping-mode with the Veeco Dimension 3100. The used cantilevers were Bruker RTESP-300 and working in the 300 kHz frequency. Room temperature magnetic hysteresis was measured by vibrating sample magnetometry (VSM; Cryogenic mCFMS-5). To evaluate the magnetic anisotropy of Mn:YIG thin films, in-plane (IP) angular resolved FMR spectra were characterized using an x-band electron spin resonance (ESR) spectrometer in the field sweeping mode with a microwave frequency of 9.5 GHz and a power of −20 dBm at various angles ϕ_H in the film plane.

Figure 1(a) shows the XRD ω-2θ scan spectra of the Mn:YIG thin films. All Mn:YIG films are epitaxially grown on GGG(111) substrates, which show predominant (444) diffraction peaks, with no diffraction peaks occurring from impurity phases or other crystallographic orientations. The root mean square (RMS) surface roughness of all Mn:YIG thin films is below 0.31 nm, as shown in the AFM images in Fig. 1(b) for YIG and Fig. 1(c) for Mn112 film, respectively. The OP lattice constant of YIG calculated from the (444) diffraction peak position is 12.438 Å, which is larger than the bulk value of 12.376 Å [8]. This lattice expansion, also reported in PLD-grown YIG films in earlier studies [18,19], are attributed to oxygen deficiency and Fe^{2+} ion generation. With increasing Mn concentrations, the OP lattice constant gradually decreases from 12.438 Å for YIG to 12.355 Å for Mn097. Considering that Mn^{3+}(0.65Å) and Fe^{3+}(0.64Å) ions show a similar ionic radius, the smaller lattice constant in Mn doped YIG thin films is possibly due to less oxygen vacancy formation with Mn doping under the same fabrication conditions due to a lower

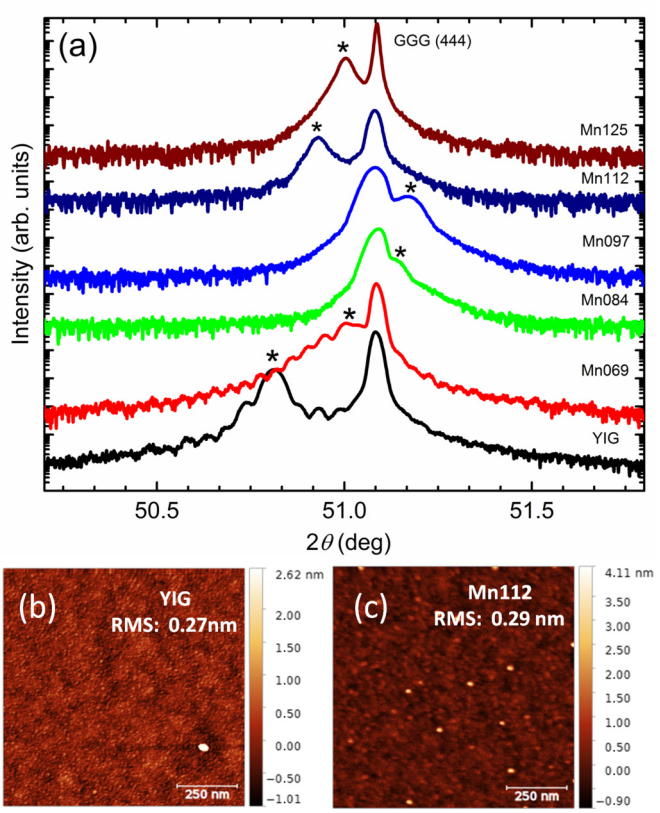

FIG. 1. (a) The XRD ω-2θ scan of Mn:YIG films with various Mn concentrations grown on GGG(111) substrate. The "✶" indicates the (444) diffraction peaks of the films. The AFM images of (b) YIG and (c) Mn112 sample surface in a 1 μm × 1 μm area. The RMS roughness of YIG and Mn112 is 0.27 nm and 0.29 nm, respectively.

equilibrium oxygen partial pressure observed in manganese oxides compared to iron oxides at the same temperature [20,21]. With further increasing of the Mn concentrations, an abrupt increase of the OP lattice constant from 12.355 Å for Mn097 to 12.412 Å for Mn112 is observed. This phenomenon can be observed when we repeat our experiments at this Mn concentration range for multiple times. It is well known that in perovskite manganites, the cooperative Jahn-Teller effect, in which percolation and long-range ordering of lattice distortion occur, can be observed in materials with high Mn concentrations [22–24]. It is possible that a similar effect is observed in our high Mn concentration doped YIG thin films grown epitaxially on GGG(111) substrate, leading to a much larger OP lattice distortion in Mn112 and Mn125 thin films. The XPS core level spectrum of the Fe and Mn $2p$ orbitals are characterized for all Mn:YIG films (see Supplement Material [25]). An abrupt peak position shift is also observed in Mn112 thin films, indicating a strong dependence of the core level binding energies to lattice distortions [29]. Since the core level spectrum peak position is both dependent on lattice distortion and the valence states, quantification of the population of different valence states for Fe and Mn ions, according to the peak positions, is not possible. However, from the $2p_{1/2}$ and satellite peak separation energies, we can infer that the Fe and Mn ions are mostly in the 3+ valence states in all films. (See discussions in the Supplemental Material and illustration in Fig. S1 [25].)

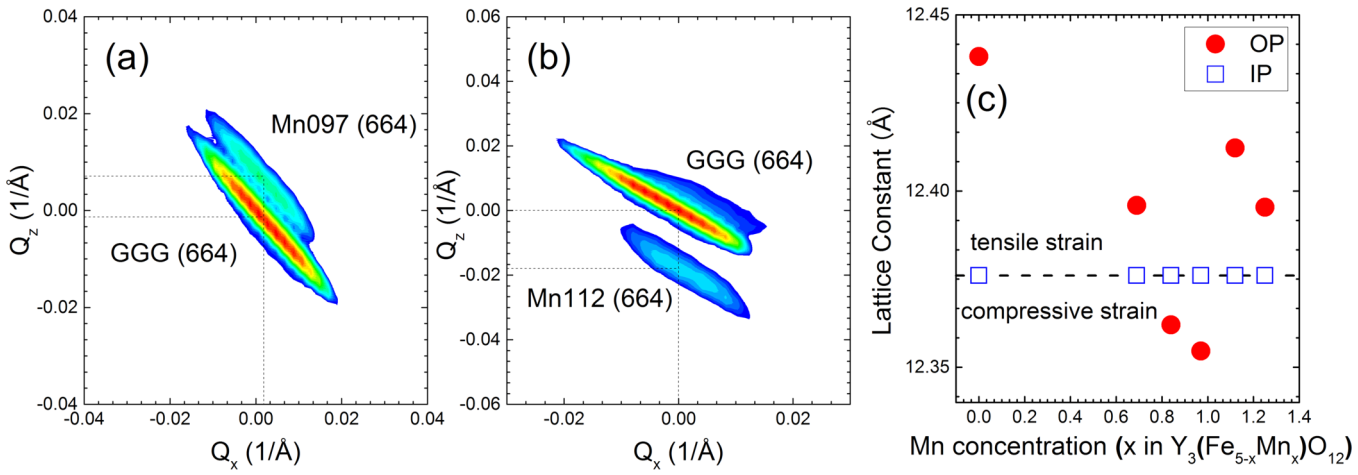

FIG. 2. (a) Reciprocal space map of the (664) diffraction peaks of Mn097 and (b) Mn112 films, respectively. (c) In-plane and out-of-plane lattice constants of Mn:YIG films.

Figures 2(a) and 2(b) show the XRD RSMs measured around the (664) substrate and film diffraction peaks for Mn097 and Mn112 samples, respectively. For both films, the IP lattice constant is identical to the substrate, indicating that both films are fully strained and coherently lattice matched to the substrate along the $[11\bar{2}]$ direction in the film plane. All other Mn:YIG thin films show similar coherent interfaces to the GGG(111) substrates from our RSM characterizations (data not shown). From these results, we calculated the IP and OP lattice constants of all Mn:YIG thin films based on the (664) and (444) diffraction peaks, as shown in Fig. 2(c). With increasing Mn concentrations, the Mn:YIG thin films show a strain state variation from an IP biaxial tensile to an IP biaxial compressive strain state. We quantify this biaxial strain as $\xi = (a_{OP} - a_{IP})/a_{IP}$, where a_{OP} and a_{IP} represent the pseudocubic lattice constant calculated from the OP lattice constant $d(444)_{OP}$ and IP lattice constant $d(11\bar{2})_{IP}$, respectively, following the equation of $d = \frac{a}{\sqrt{h^2+k^2+l^2}}$, with h, k, and l standing for the Miller indices of the crystal planes. The obtained strain values are shown in Table I, where positive and negative values indicate IP compressive and tensile strains, respectively.

To evaluate how strain influences the magnetic anisotropy of Mn:YIG thin films, we measured the room temperature hysteresis of Mn:YIG thin films in both IP and OP directions, as shown in Fig. 3. The room temperature saturation magnetization M_s of the Mn:YIG thin films first increase with Mn doping (YIG: $M_s = 133.5 \pm 5.1$ emu/cm^3; Mn069: $M_s = 139.8 \pm 4.3$ emu/cm^3), then decreases in thin films with higher Mn concentrations. This trend can be explained by Mn^{3+} preferentially occupying the octahedral site with lower magnetic moments than Fe^{3+}, which aligns antiparallel to the tetrahedral Fe^{3+} ions and yielding higher magnetization of the thin films. The Curie temperature of Mn:YIG also progressively decreases with increasing the Mn^{3+} concentration, which leads to lower M_s at room temperature for thin films with high Mn concentrations [30]. The magnetic anisotropy evolution with Mn doping can be understood qualitatively from the magnetic hysteresis. For pure YIG, the thin film shows an easy magnetization plane. The OP saturation magnetic field exceeds 2000 Oe, which is dominated by shape anisotropy and the negative magnetoelastic coefficient of Fe^{3+} ions. Due to the positive magnetoelastic coefficient in Mn^{3+} ions and the biaxial compressive strain, the magnetization process becomes harder IP and easier OP in Mn069. With further increasing of Mn concentrations to Mn084 and Mn097, the samples show magnetization easy axis IP again, which is due to their biaxial tensile strain state [see Fig. 2(c)], whereas the abrupt OP lattice distortion in Mn112 and Mn125 samples leads to drastically different magnetic hysteresis [as shown in

TABLE I. Strain and magnetic anisotropy coefficients of Mn:YIG thin films.

Samples	ξ	M_s (emu/cm^3)	H_{uni} (Oe)	H_{cub} (Oe)	$H_\perp$ (Oe)	E_{ani} (10^3 erg/cm^3)	Linewidths (Oe)	b (10^5 erg/cm^3)
YIG	0.50%	133.5 ± 5.1	-14.9 ± 0.7	-12.6 ± 1.3	-644.4 ± 8.8	43.0 ± 0.04	3.4 ± 0.1	-86.0 ± 0.08
Mn069[a]	0.16%	139.8 ± 4.3	-12.0 ± 1.1	-11.1 ± 0.8	307.5 ± 7.1	-21.5 ± 0.03	60 ± 3	134.4 ± 0.19
Mn069[b]	0.33%	139.8 ± 4.3	-9.7 ± 0.9	-15.1 ± 1.2	887.2 ± 7.5	-62.0 ± 0.03	52 ± 3	187.8 ± 0.19
Mn084	−0.09%	113.5 ± 4.5	-17.5 ± 0.8	-16.3 ± 0.8	-335.2 ± 5.3	19.0 ± 0.02	51 ± 4	211.1 ± 0.22
Mn097	−0.17%	116.2 ± 5.5	-16.7 ± 1.2	-13.9 ± 1.1	-690.9 ± 2.5	39.2 ± 0.01	30 ± 2	230.6 ± 0.06
Mn112	0.29%	125.5 ± 4.7	-14.3 ± 0.9	-14.9 ± 0.7	1337.5 ± 7.5	-82.4 ± 0.04	65 ± 3	284.1 ± 0.14
Mn125	0.16%	112.6 ± 3.5	-16.7 ± 1.0	-15.1 ± 1.1	968.6 ± 5.8	-53.3 ± 0.02	129 ± 1	333.1 ± 0.13

[a]Magnetic phase 1 in the Mn069 film, shown in Fig. S2 (see the Supplemental Material [25]).
[b]Magnetic phase 2 in the Mn069 film, shown in Fig. S2 (see the Supplemental Material [25]).

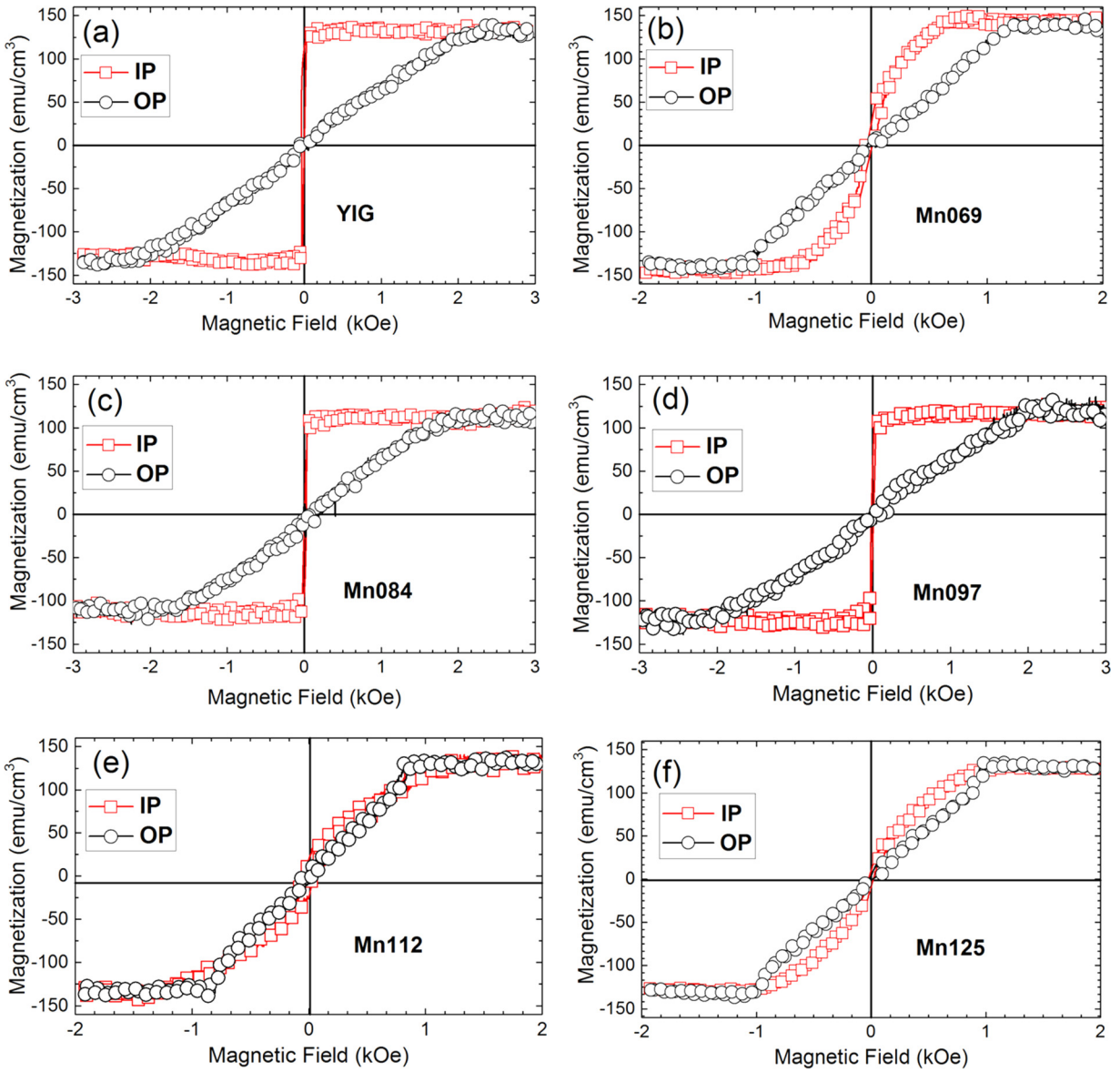

FIG. 3. Room temperature in-plane (IP) and out-of-plane (OP) magnetic hysteresis loops of Mn:YIG films: (a) YIG, (b) Mn069, (c) Mn084, (d) Mn097, (e) Mn112, and (f) Mn125.

Figs. 3(e) and 3(f), respectively]. In particular, the OP and IP magnetic saturation field of the Mn112 film is 800 Oe and 1100 Oe, respectively, indicating a weak perpendicular magnetic anisotropy in this sample caused by the large OP lattice distortion. Further enhancement of the PMA can be observed in thinner Mn112 thin films deposited on GGG(111) substrates with higher strains (see Supplemental Material Fig. S4. [25]). A dominant PMA is observed in the 30 nm thick Mn112 epitaxial thin films with a larger strain of $x = 0.82\%$.

To quantitatively determine the magnetic anisotropy constants in Mn:YIG films, IP FMR spectra were measured at room temperature. Figure 4(a) shows two representative FMR spectra of YIG and Mn112. All Mn:YIG films FMR spectra are shown in the Supplemental Material (Fig. S2) [25]. The inset of Fig. 4(a) shows the geometric configuration of the angle resolved FMR measurements. A narrow resonance linewidth of $\Delta H = 3.4$ Oe is observed in pure YIG thin films, indicating low damping and high crystal quality of this material. Due to strong spin-orbital coupling of the Mn^{3+} ions [16,17], the FMR linewidth increases with increasing Mn ion concentrations. A linewidth value of $\Delta H = 68$ Oe is observed for the Mn112 sample with PMA [as shown in Fig. 4(a)], which is still low enough for magnonic device applications [8]. The Mn:YIG films show multiple peaks in the FMR curves, indicating inhomogeneity of the magnetic phases. This inhomogeneity is possibly due to the relatively large film thickness of Mn:YIG thin films, causing strain gradients in the thin films. Besides strain inhomogeneity, the multiple peaks are likely attributable to the thickness standing spin wave modes due to the strong stress gradient along the thickness direction and/or the nonhomogeneous magnetostatic wave modes due to inhomogeneity of the RF magnetic fields. Except Mn069, the minor peaks show much

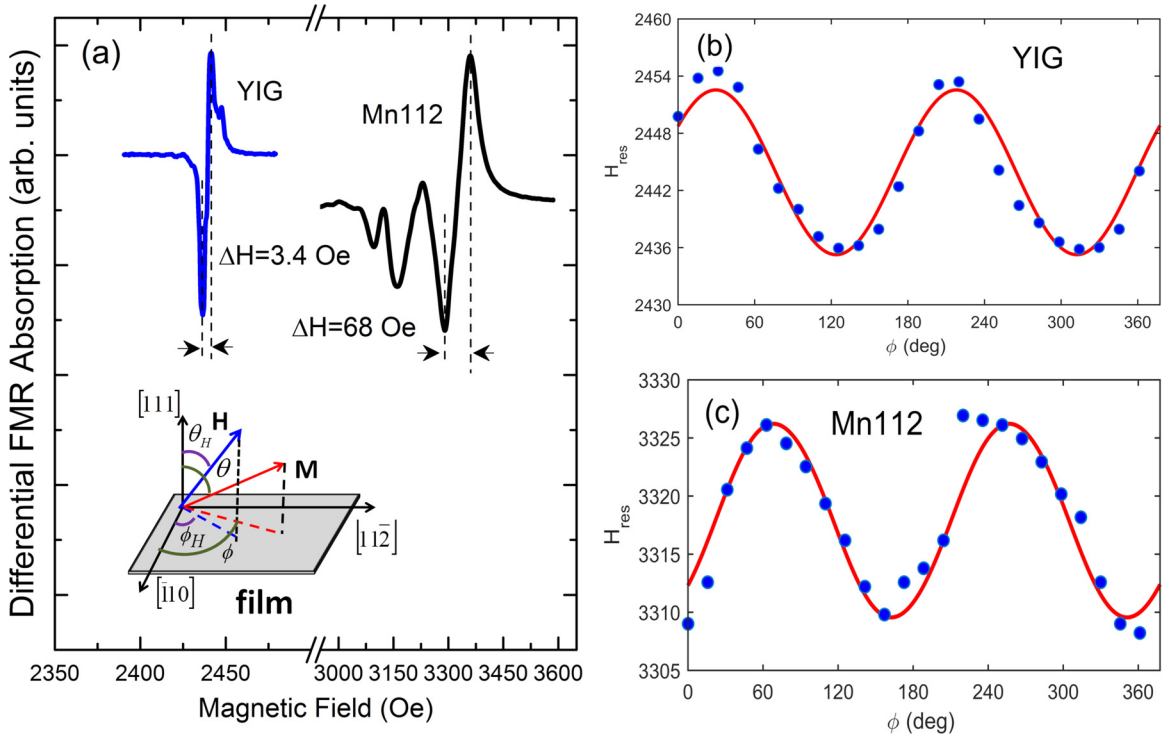

FIG. 4. (a) Room temperature in-plane FMR spectral of YIG and Mn112 films. Inset: Coordinate system for in-plane FMR analysis. In-plane angular dependence of $H_{\rm res}$ for (b) YIG and (c) Mn112 films.

weaker FMR peak intensities compared to the major phase (see Supplemental Material Fig. S2 [25]). Therefore, the strongest FMR peaks are used for the magnetic anisotropy fitting process. For Mn069, the thin film shows a strain gradient with two layers of different strain states (see Supplemental Material Fig. S3 [25]). The magnetic anisotropy fields for both layers are fitted (see Table I). The magnetic anisotropy can be determined from the expression for free energy density F of (111) orientated Mn:YIG thin films with lattice distortion [11,31]:

$$F = \frac{M_S\mu_0}{2}\Bigg[M_S\cos^2\theta - 2H(\sin\theta_H\sin\theta\cos(\phi-\phi_H)+\cos\theta\cos\phi_H) - H_{\rm uni}\sin^2\phi\sin^2\theta$$
$$- H_\perp\cos^2\theta + H_{\rm cub}\left(\frac{1}{3}-\frac{2\sin^2\theta}{3}+\frac{7\sin^4\theta}{12}+\frac{\sqrt{2}\sin 3\phi\cos\theta\sin^3\theta}{3}\right)\Bigg], \quad (1)$$

where the five terms on the right-hand side of Eq. (1) are the magnetic dipole, the Zeeman, the IP and OP uniaxial anisotropy, and the cubic anisotropy term, respectively. θ and ϕ stand for the equilibrium magnetization direction of the Mn:YIG thin films, whereas θ_H and ϕ_H are the orientation of the applied magnetic field. M_s represents the saturation magnetization of the films. H is the applied magnetic field. $H_{\rm uni}$ and $H_\perp$ are the IP and OP uniaxial anisotropy field, and $H_{\rm cub}$ is the cubic anisotropy field. The FMR frequency as a function of applied magnetic field direction is therefore derived as

$$\left(\frac{\omega}{\gamma}\right)^2 = \frac{1}{M_S^2\sin^2\theta}\left[\frac{\partial^2F}{\partial\theta^2}\frac{\partial^2F}{\partial\phi^2}-\left(\frac{\partial^2F}{\partial\theta\partial\phi}\right)^2\right], \quad (2)$$

where γ is the gyromagnetic ratio. Then, for the IP angular dependence of ϕ ($\theta=\theta_H=90^\circ$ and $\phi=\phi_H$), we obtain

$$\left(\frac{\omega}{\gamma}\right)^2 = {\mu_0}^2\Bigg[(H-H_{\rm uni}\cos 2(\phi-\phi_u))\cdot\left(H+M_S-H_\perp-\frac{H_{\rm cub}}{2}+H_{\rm uni}\sin^2(\phi-\phi_u)\right)$$
$$- H_{\rm cub}^2\frac{\cos^2 3(\phi-\phi_c)}{2}\Bigg], \quad (3)$$

where ϕu and ϕc represent the initial angle for fitting the OP uniaxial anisotropy field and cubic anisotropy field from the experiment data, respectively.

We use Eq. (3) to fit the ϕ angle resolved FMR frequencies, as shown in Figs. 4(b) and 4(c). The simulated curve matches with the measurement curves well. The measurements show a clear twofold symmetry, which is different from the expected

sixfold anisotropy in (111) oriented YIG thin films. The origin of this anisotropy may be due to a slight miscut between the substrate normal and the (111) crystal plane normal orientation, as reported in a previous study [11]. From the fitted curves, we derive H_{uni}, $H_{\perp}$, and H_{cub} using a fixed M_s determined by VSM, as shown in Table I. The OP uniaxial anisotropy field $H_{\perp}$ is observed to be strongly dependent on the Mn concentration and lattice distortion. For YIG thin films under compressive strain of $\xi = 0.50\%$, a large negative $H_{\perp} = -644.4$ Oe is observed. The negative sign of $H_{\perp}$ indicates a hard OP magnetization axis, which is consistent with the negative magnetoelastic coefficient of YIG [8,32]. This result is compared with the magnetic hysteresis loops measured by VSM shown in Fig. 3(a), where the OP saturation magnetic field $H_s^{\text{OP}} = 2290$ Oe determined by VSM is comparable to the fitted OP effective magnetic anisotropy field $H_{\text{eff}} = 4\pi M_s - H_{\perp} = 2322$ Oe from the FMR measurements. For all Mn doped YIG thin films, a reverse sign between $H_{\perp}$ and ξ is observed, indicating a dominant contribution of the positive magnetoelastic effect of Mn:YIG thin films to $H_{\perp}$ [33]. The significant strain-induced OP easy magnetization arises from the magnetoelastic effect with the change of cationic distances in the perpendicular direction, which alters the magnetic properties through spin-orbit coupling [34–36]. For fully strained pseudomorphically grown Mn:YIG(111) thin films, strain induces an OP trigonal distortion, while the IP strain is homogeneous. This explains the observed low values of the IP uniaxial anisotropy fields H_{uni}. The measured cubic anisotropy H_{cub} shows very low magnitude with no clear dependence on lattice distortions, indicating that H_{cub} is not sensitive to strain and that its magnitude is much smaller than other magnetic anisotropy fields. We also measured the angular dependent IP magnetic hysteresis loops. However, we did not observe saturation field variation within the resolution of VSM measurements (data not shown), which agrees with the weak H_{uni} and H_{cub} field determined from FMR measurements.

The magnetoelastic constant b can be derived from the magnetoelastic energy density $F = -\xi b$ when the magnetization is aligned along the film surface normal. b is related to the OP uniaxial anisotropy energy as $b = \frac{E_{\text{ani}}}{\xi} = -\frac{1}{2}\frac{M_s H_{\perp}}{\xi}$ [6,8]. The calculated b values are summarized in Table I. For pure YIG, the b value is -86.0×10^5 erg/cm^3, which agrees with previous studies well [8]. A monotonic increase of b with respect to Mn ion concentrations is observed. A large b value of 333.1×10^5 erg/cm^3 is observed in Mn125 thin films, which is about four times higher compared to YIG. These results demonstrate that Mn incorporation greatly enhances the spin-orbit coupling, which significantly boosts the capability of tuning the magnetic anisotropy by strain in YIG thin films.

In summary, we report Mn doping as an effective way to tune the magnetic anisotropy in epitaxial YIG(111) thin films. A monotonic enhancement of the magnetoelastic constant up to four times is observed with increasing Mn concentrations in Mn125 film. Tunable magnetic anisotropy is achieved in biaxially strained Mn:YIG(111) epitaxial thin films grown on GGG(111) substrates. In particular, perpendicular magnetic anisotropy is observed in Mn112 thin films, together with a narrow FMR linewidth of 65 Oe. The large tunability of magnetic anisotropy and low FMR linewidth of Mn:YIG thin films make these materials promising candidates for magnonic and magneto-optical device applications.

ACKNOWLEDGMENTS

This project is supported by the National Natural Science Foundation of China (Grants No. 61475031 and No. 51522204), the Ministry of Science and Technology of China MOST (Grant No. 2016YFA0300802), the Fundamental Research Funds for the Central Universities (Grant No. ZYGX2014Z001), and the Science Foundation for Youths of Sichuan Province (Grant No. 2015JQO014).

[1] A. D. Kent, B. Özyilmaz, and E. del Barco, Appl. Phys. Lett. **84**, 3897 (2004).
[2] D. Houssameddine, U. Ebels, B. Delaët, B. Rodmacq, I. Firastrau, F. Ponthenier, M. Brunet, C. Thirion, J. P. Michel, L. Prejbeanu-Buda, M. C. Cyrille, O. Redon, and B. Dieny, Nat. Mater. **6**, 447 (2007).
[3] J. Xiao and G. E. Bauer, Phys. Rev. Lett. **108**, 217204 (2012).
[4] O. Kamada, T. Nakaya, and S. Higuchi, Sens. Actuators A **119**, 345 (2015).
[5] X. Liu, W. L. Lim, Z. Ge, S. Shen, M. Dobrowolska, J. K. Furdyna, T. Wojtowicz, K. M. Yu, and W. Walukiewica, Appl. Phys. Lett. **86**, 112512 (2005).
[6] C. H. Du, R. Adur, H. L. Wang, A. J. Hauser, F. Y. Yang, and P. C. Hammel, Phys. Rev. Lett. **110**, 147204 (2013).
[7] C. U. Jung, H. Yamada, M. Kawasaki, and Y. Tokura, Appl. Phys. Lett. **84**, 2590 (2004).
[8] H. L. Wang, C. H. Du, P. C. Hammel, and F. Y. Yang, Phys. Rev. B **89**, 134404 (2014).
[9] E. Popova, N. Keller, F. Gendron, L. Thomas, M.-C. Brianso, M. Guyot, M. Tessier, and S. S. P. Parkin, J. Vac. Sci. Technol. A **19**, 2567 (2001).
[10] E. R. Callen, A. E. Clark, B. Desavage, W. Coleman and H. B. Callen, Phys. Rev. **130**, 1735 (1963).
[11] A. Kehlberger, K. Richter, M. C. Onbasli, G. Jakob, D. H. Kim, T. Goto, C. A. Ross, G. Götz, G. Reiss, T. Kuschel, and M. Kläui, Phys. Rev. Appl. **4**, 014008 (2015).
[12] K. Maeto, A. Itoh, S. Koike, F. Inoue, and K. Kawanishi, IEEE Trans. J. Magn. Jpn. **2**, 784 (1987).
[13] M. Kubota, A. Tsukazaki, F. Kagawa, K. Shibuya, Y. Tokunaga, M. Kawasaki, and Y. Tokura, Appl. Phys. Exp. **5**, 103002 (2012).
[14] D. Pesquera, V. Skumryev, F. Sánchez, G. Herranz, and J. Fontcuberta, Phys. Rev. B **84**, 184412 (2011).
[15] S. D. Bhame and P. A. Hoy, J. Phys. D: Appl. Phys. **40**, 3263 (2007).
[16] G. F. Dionne, IEEE Trans. Magn. **47**, 272 (2011).
[17] G. F. Dionne, J. Appl. Phys. **50**, 4263 (1979).
[18] Y. Krockenberger, H. Matsui, T. Hasegawa, M. Kawasaki, and Y. Tokura, Appl. Phys. Lett. **93**, 092505 (2008).
[19] B. M. Howe, S. Emori, H. Jeon, T. M. Oxholm, J. G. Jones, K. Mahalingam, Y. Zhuang, N. X. Sun, and G. J. Brown, IEEE Magn. Lett. **6**, 3500504 (2015).
[20] H. J. T. Elingham, J. Soc. Chem. Ind. **63**, 125 (1944).

[21] L. Bi, A. R. Taussig, H.S. Kim, L. Wang, G. F. Dionne, D. Bono, K. Persson, G. Ceder, and C. A. Ross, Phys. Rev. B **78**, 104106 (2008).
[22] B. J. Kennedy, P. J. Saines, Q. Zhou, Z. Zhang, M. Matsuda, and M. Miyake, J. Solid State Chem. **181**, 2639 (2008).
[23] V. Cuartero, J. Blasco, G. Subías, J. García, C. Meneghini, and G. Aquilanti, Phys. Rev. B **92**, 125118 (2015).
[24] S. Haw, J. Lee, S. Chen, K. Lu, M. Lee, T. Pi, C. Lee, Z. Hu and J. Chen, Dalton Trans. **45**, 12393 (2016).
[25] See Supplemental Material at http://link.aps.org/supplemental/10.1103/PhysRevB.96.224403 for XPS and FMR spectral analyses of Mn:YIG films, the RSM of the Mn069 sample, and magnetic anisotropy analysis of Mn112 films with different thicknesses, which includes Refs. [26–28].
[26] C. Wandelt, Surf. Sci. Rep. **2**, 1 (1982).
[27] E. Beyreuther, S. Grafström, L. M. Eng, C. Thiele, and K. Dörr, Phys. Rev. B **73**, 155425 (2006).
[28] J. D. Baniecki, T. Yamazaki, D. Ricinschi, Q. V. Overmeere, H. Aso, Y. Miyata, N. Fujimura, R. Maran, T. Anazawa, N. Valanoor, and Y. Imanaka, Sci. Rep. **7**, 41725 (2017).
[29] M. C. Biesinger, L. W. Lau, A. R. Gerson, and R. S. Smart, Phys. Chem. Chem. Phys. **14**, 2434 (2012).
[30] D. J. Breed, A. B. Voermans, P. Q. J. Nederpel, and B. A. H. van Bakel, J. Appl. Phys. **54**, 1519 (1983).
[31] M. Farley, Rep. Prog. Phys. **61**, 755 (1998).
[32] S. A. Manuilov, S. I. Khartsev, and A. M. Grishin, J. Appl. Phys. **106**, 123917 (2009).
[33] G. F. Dionne, IEEE Trans. Magn. **7**, 715 (1971).
[34] C. Chappert and P. Bruno, J. Appl. Phys. **64**, 5736 (1988).
[35] M. T. Johnson, P. J. H. Bolement, F. J. A. Den Broeder, and J. J. de Vries, Rep. Prog. Phys. **59**, 1409 (1996).
[36] G. F. Dionne, *Magnetic Oxides* (Springer, New York, 2009), Chap. 5.